THE ASTROPHYSICAL JOURNAL, 554:56–66, 2001 June 10

POWER SPECTRUM COVARIANCE OF WEAK GRAVITATIONAL LENSING

ASANTHA COORAY AND WAYNE HU
Department of Astronomy and Astrophysics, University of Chicago, 5640 South Ellis Avenue, Chicago, IL 60637;
asante@hyde.uchicago.edu, whu@background.uchicago.edu
Received 2000 December 5; accepted 2001 February 8

ABSTRACT

Weak gravitational lensing observations probe the spectrum and evolution of density fluctuations and the cosmological parameters that govern them. At low redshifts, the nonlinear gravitational evolution of large-scale structure produces a non-Gaussian covariance in the shear power spectrum measurements that affects their translation into cosmological parameters. Using the dark matter halo approach, we study the covariance of binned band power spectrum estimates and the four-point function of the dark matter density field that underlies it. We compare this semianalytic estimate to results from N-body numerical simulations and find good agreement. We find that for a survey out to $z \sim 1$, the power spectrum covariance increases the errors on cosmological parameters determined under the Gaussian assumption by about 15%.

Subject headings: cosmology: theory — gravitational lensing — large-scale structure of universe

1. INTRODUCTION

Weak gravitational lensing by large-scale structure (LSS) shears the images of faint galaxies at the percent level and correlates their measured ellipticities (e.g., Blandford et al. 1991; Miralda-Escudé 1991; Kaiser 1992). Although challenging to measure, the two-point correlations, and the power spectrum that underlies them, provide important cosmological information that is complementary to that supplied by the cosmic microwave background, and potentially as precise (e.g., Jain & Seljak 1997; Bernardeau, van Waerbeke, & Mellier 1997; Kaiser 1998; Hu & Tegmark 1999; Hui 1999; Cooray 1999; Van Waerbeke, Bernardeau, & Mellier 1999; see Bartelmann & Schneider 2001 for a recent review). Indeed, several recent studies have provided the first clear evidence for weak lensing in so-called blank fields, where the large-scale structure signal is expected to dominate (e.g., Van Waerbeke et al. 2000; Bacon, Refregier, & Ellis 2000; Wittman et al. 2000; Kaiser, Wilson, & Luppino 2000).

Given that weak gravitational lensing probes the projected mass distribution, its statistical properties reflect those of the dark matter. Nonlinearities in the mass distribution, due to gravitational evolution at low redshifts, cause the shear field to become non-Gaussian. It is well known that lensing induces a measurable three-point correlation in the derived convergence field (Bernardeau et al. 1997; Cooray & Hu 2001). The same processes also induce a four-point correlation. The four-point correlations are of particular interest in that they quantify the sample variance and covariance of two-point correlation or power spectrum measurements. Previous studies of the ability of power spectrum measurements to constrain cosmology have been based on a Gaussian approximation to the sample variance and the assumption that covariance is negligible (e.g., Hu & Tegmark 1999); it is of interest to test to what extent their inferences remain valid in the presence of realistic non-Gaussianity. More importantly, when interpreting the power spectrum recovered from the next generation of surveys, an accurate propagation of errors will be critical (Hu & White 2000).

Here we present a semianalytical estimate of the Fourier analog of the four-point function, i.e., the trispectrum, and calculate in detail the configurations that contribute to power spectrum covariance. Since weak-lensing shear and convergence can be written as a simple projection of the dark matter density field, the problem reduces to a study of the trispectrum of the density field. Previous studies of the dark matter trispectrum have employed a mix of perturbation theory and nonlinear scalings (e.g., Scoccimarro, Zaldarriaga, & Hui 1999) or N-body simulations (Meiksin & White 1999). The former are not applicable to the full range of scales and configurations of interest; the latter are limited by computational expense to a handful of realizations of cosmological models with modest dynamical range.

Here we use the dark matter halo approach to model the density field (Seljak 2000; Ma & Fry 2000a; Scoccimarro et al. 2001) and extend our previous treatments of the two- and three-point lensing statistics (Cooray, Hu, & Miralda-Escudé 2000; Cooray & Hu 2001). The critical ingredients are: a mass function for the halo distribution, such as the Press-Schechter (PS; Press & Schechter 1974) mass function; a profile for the dark matter halo, e.g., the profile of Navarro, Frenk, & White (1996; NFW), and a description of halo biasing (Mo, Jing, & White 1997). In the mildly nonlinear regime, where most of the contribution to lensing is expected, the accuracy of the halo model has been extensively tested against simulations at the two- and three-point levels (Seljak 2000; Ma & Fry 2000a; Scoccimarro et al. 2001). We present tests here of the four-point configurations involved in the power spectrum covariance. These techniques can also be extended to the covariance of the power spectrum of galaxy redshift surveys with a prescription for assigning galaxies to halos (Seljak 2000; Scoccimarro et al. 2001). The effect of non-Gaussianities on the measured galaxy power spectrum, through a measurement of the angular correlation function, is discussed in Eisenstein & Zaldarriaga (2001).

In § 2, we study the trispectrum of the dark matter density field under the halo model and test it against simulations from Meiksin & White (1999). In § 3, we apply these techniques to the weak-lensing covariance and test them against the simulations of White & Hu (2000). We also discuss the effect of power spectrum covariance on cosmological parameter estimation.

2. DARK MATTER POWER SPECTRUM COVARIANCE

We begin by defining the power spectrum, trispectrum, and power spectrum covariance in § 2.1. We then derive the halo model for these quantities in § 2.2. In § 2.3, we present results and comparisons with N-body simulations.

2.1. *General Definitions*

The two- and four-point correlations of the density field are defined in the usual way,

$$\langle \delta(\boldsymbol{k}_1)\delta(\boldsymbol{k}_2)\rangle = (2\pi)^3\delta_{\rm D}(\boldsymbol{k}_{12})P(k_1)\,, \tag{1}$$

$$\langle \delta(\boldsymbol{k}_1)\ldots\delta(\boldsymbol{k}_4)\rangle_c = (2\pi)^3\delta_{\rm D}(\boldsymbol{k}_{1234})T(\boldsymbol{k}_1, \boldsymbol{k}_2, \boldsymbol{k}_3, \boldsymbol{k}_4)\,, \tag{2}$$

where $\boldsymbol{k}_{i\ldots j} = \boldsymbol{k}_i + \ldots + \boldsymbol{k}_j$, and $\delta_{\rm D}$ is the delta function, not to be confused with the density perturbation. Note that the subscript c denotes the connected piece, i.e., the trispectrum is defined to be identically zero for a Gaussian field. Here and throughout, we occasionally suppress the redshift dependence where no confusion will arise.

Because of the closure condition expressed by the delta function, the trispectrum can be viewed as a four-sided figure with sides $\boldsymbol{k}_i$. It can alternately be described by the length of the four sides k_i plus the diagonals. We occasionally refer to elements of the trispectrum that differ by the length of the diagonals as different configurations of the trispectrum.

Following Scoccimarro et al. (1999), we can relate the trispectrum to the variance of the estimator of the binned power spectrum,

$$\hat{P}_i = \frac{1}{V}\int_{s,i}\frac{d^3k}{V_{s,i}}\,\delta^*(-\boldsymbol{k})\delta(\boldsymbol{k})\,, \tag{3}$$

where the integral is over a shell in k-space centered around k_i, $V_{s,i} \approx 4\pi k_i^2\,\delta k$ is the volume of the shell, and V is the volume of the survey. Recalling that $\delta(0) \to V/(2\pi)^3$ for a finite volume,

$$\begin{aligned} C_{ij} &\equiv \langle \hat{P}_i\hat{P}_j\rangle - \langle\hat{P}_i\rangle\langle\hat{P}_j\rangle \\ &= \frac{1}{V}\left[\frac{(2\pi)^3}{V_{s,i}}\,2P_i^2\,\delta_{ij} + T_{ij}\right], \end{aligned} \tag{4}$$

where

$$T_{ij} \equiv \int_{s,i}\frac{d^3k_i}{V_{s,i}}\int_{s,j}\frac{d^3k_j}{V_{s,j}}\,T(\boldsymbol{k}_i, -\boldsymbol{k}_i, \boldsymbol{k}_j, -\boldsymbol{k}_j)\,. \tag{5}$$

Note that although both terms scale in the same way with the volume of the survey, only the Gaussian piece necessarily decreases with the volume of the shell. For the Gaussian piece, the sampling error reduces to a simple root-N mode counting of independent modes in a shell. The trispectrum quantifies the nonindependence of the modes both within a shell and between shells. Calculating the covariance matrix of the power spectrum estimates reduces to averaging the elements of the trispectrum across configurations in the shell. We now turn to the subject of modeling the trispectrum.

2.2. *Halo Model*

We model the power spectrum and trispectrum of the dark matter field under the halo approach. Here we present in detail the extensions required to model the trispectrum. We refer the reader to Cooray & Hu (2001) for a more in-depth treatment of the components.

The halo approach models the fully nonlinear dark matter density field as a set of correlated discrete objects ("halos") with profiles ρ_i that for definiteness depend on their mass M and concentration c as in the NFW profile (Navarro et al. 1996),[1]

$$\rho(\boldsymbol{x}) = \sum_i \rho_h(\boldsymbol{x} - \boldsymbol{x}_i;\, M_i,\, c_i)\,, \tag{6}$$

where the sum is over all positions. The density fluctuation in Fourier space is

$$\delta(\boldsymbol{k}) = \sum_i e^{i\boldsymbol{k}\cdot\boldsymbol{x}_i}\delta_h(\boldsymbol{k};\, M_i;\, c_i)\,. \tag{7}$$

Following Peebles (1980), let us divide up space into sufficiently small volumes δV that they contain only one or zero halos of a given mass and concentration and convert the sum over halos to a sum over the volume elements, masses, and concentrations,

$$\delta(\boldsymbol{k}) = \sum_{V_1, M_1, c_1} n_1\, e^{i\boldsymbol{k}\cdot\boldsymbol{x}_1}\delta_h(\boldsymbol{k},\, M_1,\, c_1)\,. \tag{8}$$

By virtue of the small volume element, $n_1 = n_1^2 = n_1^\mu = 1$ or 0, following Peebles (1980).

The final component is that the halos themselves are taken to be biased tracers of the *linear* density field (denoted by "pt"),[2] such that their number density fluctuates as

$$\frac{d^2n}{dM\,dc}(\boldsymbol{x}) = \frac{d^2\bar{n}}{dM\,dc}\left[b_0 + b_1(M)\delta_{\rm pt}(\boldsymbol{x}) + \frac{1}{2}\,b_2(M)\delta_{\rm pt}^2(\boldsymbol{x})\ldots\right], \tag{9}$$

where $b_0 \equiv 1$, and the halo bias parameters are given in Mo et al. (1997). Thus,

$$\langle n_1\rangle = \frac{d^2\bar{n}}{dMdc}\,\delta M_1\,\delta c_1\,, \tag{10}$$

$$\begin{aligned} \langle n_1\, n_2\rangle &= \langle n_1\rangle^2\delta_{12} + \langle n_1\rangle\langle n_2\rangle[b_0^2 + b_1(M_1) \\ &\quad \times b_1(M_2)\langle\delta_{\rm pt}(\boldsymbol{x}_1)\delta_{\rm pt}(\boldsymbol{x}_2)\rangle]\,, \end{aligned}$$

$$\langle n_1\, n_2\, n_3\rangle = \ldots\,. \tag{11}$$

The derivation of the higher point functions in Fourier space is now a straightforward but tedious exercise in algebra. The Fourier transforms inherent in equation (8) convert the correlation functions in equation (11) into the power spectrum, bispectrum, trispectrum, etc., of perturbation theory.

Replacing sums with integrals, we obtain expressions based on the general integral

$$\begin{aligned} I_\mu^\beta(k_1,\ldots,k_\mu) &\equiv \int dM\int dc\,\frac{d^2\bar{n}}{dMdc}\,b_\beta(M) \\ &\quad \times \delta_h(k_1,\, M,\, c)\ldots\delta_h(k_\mu,\, M,\, c)\,. \end{aligned} \tag{12}$$

The index μ represents the number of points taken to be in the same halo, such that $\langle n_1^\mu\rangle = \langle n_1\rangle$.

[1] This prescription can be generalized for more complicated halo profiles in the obvious way.

[2] It should be understood that "pt" here denotes the lowest nonvanishing order of perturbation theory for the object in question. For the power spectrum, this is linear perturbation theory; for the bispectrum, this is second-order perturbation theory, etc.

The power spectrum under the halo model becomes (Seljak 2000)

$$P(k) = P^{1h}(k) + P^{2h}(k) , \quad (13)$$

$$P^{1h}(k) = I_2^0(k, k) , \quad (14)$$

$$P^{2h}(k) = [I_1^1(k)]^2 P^{pt}(k) , \quad (15)$$

where the two terms represent contributions from two points in a single halo (1h) and points in different halos (2h), respectively.

Likewise, for the trispectrum, the contributions can be separated into those involving one to four halos,

$$T = T^{1h} + T^{2h} + T^{3h} + T^{4h} , \quad (16)$$

where here and below the argument of the trispectrum is understood to be $(\boldsymbol{k}_1, \boldsymbol{k}_2, \boldsymbol{k}_3, \boldsymbol{k}_4)$. The term involving a single halo probes correlations of dark matter within that halo,

$$T^{1h} = I_4^0(k_1, k_2, k_3, k_4) , \quad (17)$$

and is independent of configuration because of the assumed spherical symmetry for our halos.

The term involving two halos can be further broken up into two parts,

$$T^{2h} = T_{31}^{2h} + T_{22}^{2h} , \quad (18)$$

which represent taking three or two points in the first halo,

$$T_{31}^{2h} = P^{pt}(k_1) I_3^1(k_2, k_3, k_4) I_1^1(k_1) + 3 \text{ perm.} , \quad (19)$$

$$T_{22}^{2h} = P^{pt}(k_{12}) I_2^1(k_1, k_2) I_2^1(k_3, k_4) + 2 \text{ perm} . \quad (20)$$

The permutations involve the three other choices of k_i for the I_1^1 term in the first equation, and the two other pairings of the k_i for the I_2^1 terms in the second. Here we define $\boldsymbol{k}_{12} = \boldsymbol{k}_1 + \boldsymbol{k}_2$; note that k_{12} is the length of one of the diagonals in the configuration.

The term containing three halos can only arise with two points in one halo and one in each of the others,

$$T^{3h} = B^{pt}(\boldsymbol{k}_1, \boldsymbol{k}_2, \boldsymbol{k}_{34}) I_2^1(k_3, k_4) I_1^1(k_1) I_1^1(k_2) + P^{pt}(k_1) P^{pt}(k_2) I_2^2(k_3, k_4) I_1^1(k_1) I_1^1(k_2) + 5 \text{ perm.} , \quad (21)$$

where the permutations represent the unique pairings of the k_i in the I_2 factors. This term also depends on the configuration. The bispectrum in perturbation theory is given by[3]

$$B^{pt}(\boldsymbol{k}_p, \boldsymbol{k}_q, \boldsymbol{k}_r) = 2F_2^s(\boldsymbol{k}_p, \boldsymbol{k}_q) P(k_p) P(k_q) + 2 \text{ perm.} , \quad (22)$$

where the F_2^s term is given by second-order gravitational perturbation calculations (see below).

Finally for four halos, the contribution is

$$T^{4h} = I_1^1(k_1) I_1^1(k_2) I_1^1(k_3) I_1^1(k_4) \left\{ T^{pt} + \left[\frac{I_2^1(k_4)}{I_1^1(k_4)} \times P^{pt}(k_1) P^{pt}(k_2) P^{pt}(k_3) + 3 \text{ perm.} \right] \right\} , \quad (23)$$

where the permutations represent the choice of k_i in the I^1 in the brackets. The perturbation trispectrum can be written as (Fry 1984)

$$T^{pt} = 4[F_2^s(\boldsymbol{k}_{12}, -\boldsymbol{k}_1) F_2^s(\boldsymbol{k}_{12}, \boldsymbol{k}_3) P(k_1) \times P(k_{12}) P(k_3) + \text{perm.}] + 6[F_3^s(\boldsymbol{k}_1, \boldsymbol{k}_2, \boldsymbol{k}_3) P(k_1) P(k_2) P(k_3) + \text{perm.}] . \quad (24)$$

The permutations involve a total of 12 terms in the first set and four terms in the second set. We now discuss the results from this modeling for a specific choice of halo input parameters and cosmology.

2.3. *Results*

2.3.1. *Fiducial Model*

We evaluate the trispectrum under the halo model of the last section assuming an NFW profile for the halos (Navarro et al. 1996), which depends on their virial mass M and concentration c. For the differential number density we take

$$\frac{d\bar{n}}{dM\, dc} = \left(\frac{dn}{dM} \right)_{PS} p(c) , \quad (25)$$

$$p(c)dc = \frac{1}{\sqrt{2\pi\sigma_c^2}} \exp\left[-\frac{(\ln c - \ln \bar{c})^2}{2\sigma_{\ln c}^2} \right] d\ln c ,$$

where PS denotes the Press-Schechter mass function. From the simulations of Bullock et al. (2001), the mean and width of the concentration distribution is taken to be

$$\bar{c}(M, z) = 9(1 + z)^{-1} \left[\frac{M}{M_*(z)} \right]^{-0.13} , \quad (26)$$

$$\sigma_{\ln c} = 0.2 , \quad (27)$$

where $M_*(z)$ is the nonlinear mass scale at which the peak-height threshold $\nu(M, z) = 1$.

This prescription differs from that in Cooray & Hu (2001) where $\sigma_{\ln c} \to 0$, since a finite distribution becomes increasingly important for the higher moments. To maintain consistency, we have also taken the mean concentration directly from simulations, rather than empirically adjusting it to match the power spectrum. For the same reason we choose a ΛCDM cosmological model with $\Omega_m = 0.3$, $\Omega_\Lambda = 0.7$, $h = 0.65$, and a scale-invariant spectrum of primordial fluctuations. This model has mass fluctuations on the 8 h Mpc^{-1} scale of ~ 1.0, consistent with the abundance of galaxy clusters (Viana & Liddle 1999) and *COBE* (Bunn & White 1997). For the linear power spectrum, we take the fitting formula for the transfer function given in Eisenstein & Hu (1999).

2.3.2. *Comparisons*

In Figure 1*a*, we show the logarithmic power spectrum $\Delta^2(k) = k^3 P(k)/2\pi^2$ with contributions broken down to the 1h and 2h terms today and the 1h term at a redshift of 1. We find that there is an slight overprediction of power at scales corresponding to $1 \lesssim k \lesssim 10\ h$ Mpc^{-1} when compared to the Peacock & Dodds (1996, hereafter PD) fitting function shown for redshifts of 0 and 1, and a more substantial underprediction at small scales with $k \gtrsim 10\ h$ Mpc^{-1}. Since the nonlinear power spectrum has only been properly studied out to overdensities $\Delta^2 \sim 10^3$ with numerical simu-

[3] The kernels F_n^s are derived in Goroff et al. (1986; see their eqs. [A2] and [A3]; note that their $P_n \equiv F_n$), and we have written it such that the symmetric form of F_n are used. The use of the symmetric form accounts for the factor of 2 in equation (22) and factors of 4 and 6 in equation (24).

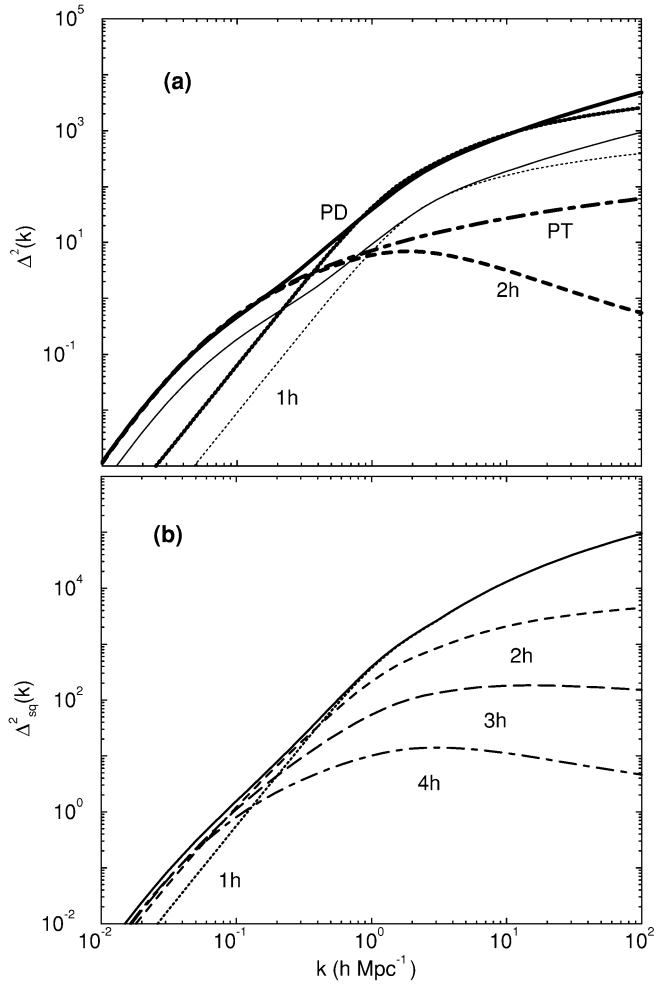

FIG. 1.—(*a*) Dark matter power spectrum and (*b*) square-configuration trispectrum, broken into individual contributions under the halo description. The lines labeled "PD" shows the dark matter power spectrum under the Peacock & Dodds (1996) nonlinear fitting function, while the curve labeled "PT" shows the linear dark matter power spectrum (at redshift of 0). In (*a*), we show the power spectrum at redshifts of 0 and 1. In (*b*), we show the square configuration trispectrum (see text). In both (*a*) and (*b*), at small scales the single halo term dominates, while at large scales halo correlations contribute.

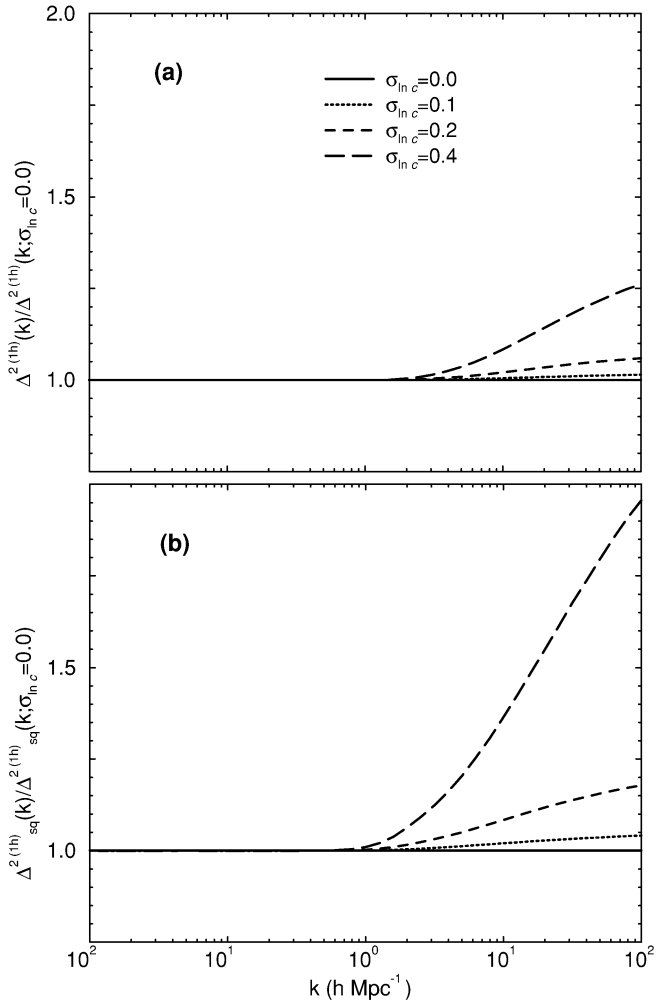

FIG. 2.—Ratio of the single halo term contribution to that for a concentration width $\sigma_{\ln c} \to 0$ for the (*a*) power spectrum and (*b*) trispectrum. The small-scale behavior is increasingly sensitive to the high-concentration tails for the higher order statistics.

lations, it is unclear whether the small-scale disagreement is significant. Fortunately, it is on sufficiently small scales so as not to affect the lensing observables.

For the trispectrum, we are mainly interested in terms involving $T(\boldsymbol{k}_1, -\boldsymbol{k}_1, \boldsymbol{k}_2, -\boldsymbol{k}_2)$, i.e., parallelograms that are defined by either the length k_{12} or the angle between $\boldsymbol{k}_1$ and $\boldsymbol{k}_2$. For illustration purposes, we take $k_1 = k_2$ and the angle to be 90° ($\boldsymbol{k}_2 = \boldsymbol{k}_\perp$), such that the parallelogram is a square. It is then convenient to define

$$\Delta^2_{\rm sq}(k) \equiv \frac{k^3}{2\pi^2}\, T^{1/3}(\boldsymbol{k}, -\boldsymbol{k}, \boldsymbol{k}_\perp, -\boldsymbol{k}_\perp)\,, \tag{28}$$

such that this quantity scales roughly as the logarithmic power spectrum itself, $\Delta^2(k)$. This spectrum is shown in Figure 1*b* with the individual contributions from the 1h, 2h, 3h, and 4h terms shown. We test the sensitivity of our calculations to the width of the distribution in Figure 2, where we show the ratio between the single-halo contribution, as a function of the concentration distribution width, to the halo term with a delta function distribution, $\sigma_c = 0$. As in the power spectrum, the effect of increasing the width is to increase the amplitude at small scales due to the high-concentration tail of the distribution. Note that the width effect is stronger in the trispectrum than the power spectrum, since the tails of the distribution are weighted more heavily in higher point statistics.

To compare the specific scaling predicted by perturbation theory in the linear regime and the hierarchical *Ansatz* in the deeply nonlinear regime, it is useful to define the quantity

$$Q_{\rm sq}(k) \equiv \frac{T(\boldsymbol{k}, -\boldsymbol{k}, \boldsymbol{k}_\perp, -\boldsymbol{k}_\perp)}{[8P^2(k)P(\sqrt{2}k)][4P^3(k)]}\,. \tag{29}$$

In the halo prescription, $Q_{\rm sq}$ at $k \gtrsim 10k_{\rm nonlin} \sim 10\ h\ {\rm Mpc}^{-1}$ arises mainly from the single-halo term. In perturbation theory, $Q_{\rm sq} \approx 0.085$. The $Q_{\rm sq}$ does not approach the perturbation theory prediction as $k \to 0$, since that contribution appears only as one term in the four-halo piece. Our model therefore does not recover the true trispectrum of the density field in the linear regime. The problem is that in modeling the density field with discrete objects (here halos), there is an error associated with shot noise. A more familiar

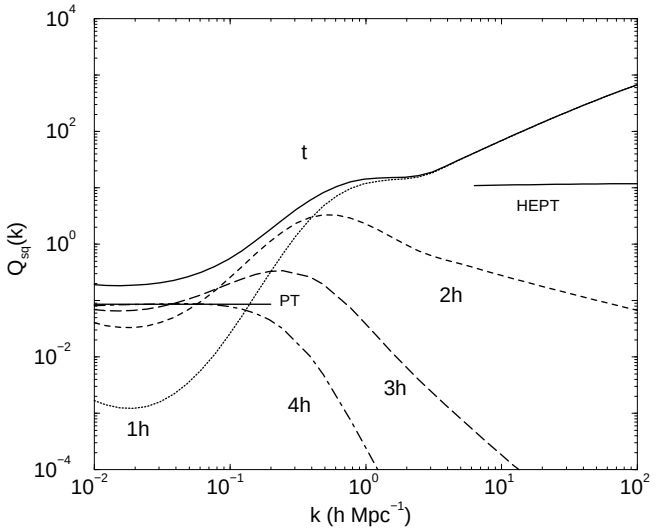

FIG. 3.—Q_{sq} at present, broken into individual contributions under the halo description. The hierarchical model predicts a constant value for Q_{sq} in the deeply nonlinear regime for clustering (HEPT). In the linear regime, the perturbation theory (PT) prediction is reproduced by the four-halo term, which is only $\sim\frac{1}{2}$ of the total. See text for a discussion of discrepancies.

example of the same effect comes from the use of galaxies as tracers of the dark matter density field. While this error appears large in the Q_{sq} statistic, it does not affect the calculations of the power spectrum covariance, since in this regime it is the Gaussian piece errors that dominate.

The hierarchical *Ansatz* predicts that $Q_{sq} = \text{const}$ in the deeply nonlinear regime. Its value is unspecified by the *Ansatz*, but is given as

$$Q_{sq}^{sat} = \frac{1}{2}\left[\frac{54 - 27\times 2^n + 2\times 3^n + 6^n}{1 + 6\times 2^n + 3\times 3^n + 6\times 6^n}\right] \qquad (30)$$

under hyperextended perturbation theory (HEPT; Scoccimarro & Frieman). Here $n = n(k)$ is the linear power spectral index at k. As shown in Figure 3, the halo model predicts that Q_{sq} increases at high k. This behavior, also present at the three-point level for the dark matter density field bispectrum, suggests disagreement between the halo approach and the hierarchical clustering *Ansatz* (see Ma & Fry 2000b), although numerical simulations do not yet have enough resolution to test this disagreement. Fortunately, the discrepancy is also outside the regime important for lensing.

To further test the accuracy of our halo trispectrum, we compare dark matter correlations predicted by our method to those from numerical simulations by Meiksin & White (1999). For this purpose, we calculate the covariance matrix C_{ij} from equation (5) with the bins centered at k_i and volume $V_{s,i} = 4\pi k_i^2\,\delta k_i$ corresponding to their scheme. We also employ the parameters of their ΛCDM cosmology and assume that the parameters that defined the halo concentration properties from our fiducial ΛCDM model holds for this cosmological model also. The physical differences between the two cosmological models are minor, although normalization differences can lead to large changes in the correlation coefficients.

In Table 1, we compare the predictions for the correlation coefficients

$$\hat{C}_{ij} = \frac{C_{ij}}{\sqrt{C_{ii}\,C_{jj}}} \qquad (31)$$

with the simulations. Agreement in the off-diagonal elements is typically better than ± 0.1, even in the region where non-Gaussian effects dominate, and the qualitative features such as the increase in correlations across the nonlinear scale are preserved.

A further test of the accuracy of the halo approach is to consider higher order real-space moments, such as skewness and kurtosis. In Cooray & Hu (2001), we discussed the weak-lensing convergence skewness under the halo model and found it to be in agreement with numerical predictions from White & Hu (2000). The fourth moment of the density field, under certain approximations, was calculated by Scoccimarro et al. (1999) using dark matter halos and was found to be in good agreement with N-body simulations. Given that density field moments have already been studied by Scoccimarro, Zaldarriaga, & Hui, we no longer consider them here other than to suggest that the halo model has provided, at least qualitatively, a consistent description that is better than any of the perturbation theory arguments.

TABLE 1

DARK MATTER POWER SPECTRUM CORRELATIONS

k	0.031	0.044	0.058	0.074	0.093	0.110	0.138	0.169	0.206	0.254	0.313	0.385
0.031	1.000	0.019	0.041	0.065	0.086	0.113	0.149	0.172	0.186	0.186	0.172	0.155
0.044	(−0.017)	1.000	0.036	0.075	0.111	0.153	0.204	0.238	0.261	0.264	0.251	0.230
0.058	(0.023)	(0.001)	1.000	0.062	0.118	0.183	0.255	0.302	0.334	0.341	0.328	0.305
0.074	(0.024)	(0.024)	(0.041)	1.000	0.102	0.189	0.299	0.368	0.412	0.425	0.412	0.389
0.093	(0.042)	(0.056)	(0.027)	(0.079)	1.000	0.160	0.295	0.404	0.466	0.485	0.475	0.453
0.110	(0.154)	(0.076)	(0.086)	(0.094)	(0.028)	1.000	0.277	0.433	0.541	0.576	0.570	0.549
0.138	(0.176)	(0.118)	(0.149)	(0.202)	(0.085)	(0.205)	1.000	0.434	0.580	0.693	0.698	0.680
0.169	(0.188)	(0.180)	(0.138)	(0.229)	(0.177)	(0.251)	(0.281)	1.000	0.592	0.737	0.778	0.766
0.206	(0.224)	(0.165)	(0.177)	(0.322)	(0.193)	(0.314)	(0.396)	(0.484)	1.000	0.748	0.839	0.848
0.254	(0.264)	(0.228)	(0.206)	(0.343)	(0.261)	(0.355)	(0.488)	(0.606)	(0.654)	1.000	0.858	0.896
0.313	(0.265)	(0.234)	(0.202)	(0.374)	(0.259)	(0.397)	(0.506)	(0.618)	(0.720)	(0.816)	1.000	0.914
0.385	(0.270)	(0.227)	(0.205)	(0.391)	(0.262)	(0.374)	(0.508)	(0.633)	(0.733)	(0.835)	(0.902)	1.000
$\sqrt{C_{ii}/C^G_{ii}}$	1.00	1.01	1.02	1.03	1.04	1.07	1.14	1.23	1.38	1.61	1.90	2.26

NOTE.—Diagonal normalized covariance matrix of the binned dark matter density field power spectrum with k values in units of h Mpc^{-1}. Upper triangle displays the covariance found under the halo model. Lower triangle (parenthetical numbers) displays the covariance found in numerical simulations by Meiksin & White (1999). Bottom row shows the fractional increase in the errors (root diagonal covariance) due to non-Gaussianity, as calculated under the halo model.

Even though the dark matter halo formalism provides a physically motivated means of calculating the statistics of the dark matter density field, and especially higher order correlations, there are several limitations of this approach that should be borne in mind when interpreting results. This approach assumes that all halos share a parameterized spherically symmetric profile. We have attempted to include variations in the halo profiles with the addition of a distribution function for the concentration parameter based on results from numerical simulations. Unlike our previous calculations presented in Cooray et al. (2000) and Cooray & Hu (2001), we have not modified the concentration-mass relation to fit the PD nonlinear power spectrum, but rather have taken results directly from simulations as inputs. Although we have partly accounted for halo profile variations, the assumption that halos are spherical is likely to affect detailed results on the configuration dependence of the trispectrum.

Since we are considering a weighted average of configurations, our tests presented here and other work through simulations are insufficient to establish the validity of the trispectrum modeling in general. Further numerical work is required to quantify to what extent the present approach reproduces simulation results for the full trispectrum.

For reference, in the case of the density field bispectrum, Scoccimarro et al. (2001) found discrepancies at the $\sim 20\%$–30% level in the mildly nonlinear regime in the configuration dependence. When averaged over configurations, Ma & Fry (2000a) found that predictions of the halo formalism are in good agreement with simulations. They also showed that the power spectrum and bispectrum in the simulations can be adequately modeled with the replacement of real halos with smooth, spherical NFW profiles by Ma & Fry (2000b). This level of agreement in the bispectrum leads one to hope that the configuration dependence of the trispectrum is not severely affected by asphericity, mergers, and substructure, at least in the moderately nonlinear regime.

3. CONVERGENCE POWER SPECTRUM COVARIANCE

3.1. *General Definitions*

Weak lensing probes the statistical properties of the shear field on the sky, which is a weighted projection of the matter distribution along the line of sight to the source galaxies. As such, the observables can be reexpressed as a scalar quantity, the convergence κ, on the sky.

Its power spectrum and trispectrum are defined in the flat-sky approximation in the usual way,

$$\langle \kappa(\boldsymbol{l}_1)\kappa(\boldsymbol{l}_2)\rangle = (2\pi)^2\delta_{\rm D}(\boldsymbol{l}_{12})C_l^\kappa\,,$$
$$\langle \kappa(\boldsymbol{l}_1)\ldots\kappa(\boldsymbol{l}_4)\rangle_c = (2\pi)^2\delta_{\rm D}(\boldsymbol{l}_{1234})T^\kappa(\boldsymbol{l}_1,\boldsymbol{l}_2,\boldsymbol{l}_3,\boldsymbol{l}_4)\,. \quad (32)$$

These are related to the density power spectrum and trispectrum by the projections (Kaiser 1992; Scoccimarro et al. 1999)

$$C_l^\kappa = \int dr\,\frac{W(r)^2}{d_A^2}\,P\!\left(\frac{l}{d_A};r\right), \quad (33)$$

$$T^\kappa = \int dr\,\frac{W(r)^4}{d_A^6}\,T\!\left(\frac{\boldsymbol{l}_1}{d_A},\frac{\boldsymbol{l}_2}{d_A},\frac{\boldsymbol{l}_3}{d_A},\frac{\boldsymbol{l}_4}{d_A};r\right), \quad (34)$$

where r is the comoving distance and d_A is the angular diameter distance. When all background sources are at a distance of r_s, the weight function becomes

$$W(r) = \frac{3}{2}\,\Omega_m\,\frac{H_0^2}{c^2 a}\,\frac{d_A(r)d_A(r_s-r)}{d_A(r_s)}\,; \quad (35)$$

for simplicity, we assume $r_s = r(z_s = 1)$. In deriving equation (34), we have used the Limber approximation (Limber 1954) by setting $k = l/d_A$ and the flat-sky approximation. A potential problem in using the Limber approximation is that we implicitly integrate over the unperturbed photon paths (Born approximation). The Born approximation has been tested in numerical simulations by Jain et al. (2000; see their Fig. 7) and found to be an excellent approximation for the two-point statistics. The same approximation can also be tested through lens-lens coupling involving lenses at two different redshifts. For higher order correlations, analytical calculations in the mildly nonlinear regime by Van Waerbeke et al. (2001; see also Bernardeau et al. 1997; Schneider et al. 1998) indicate that corrections are again less than a few percent. Thus, our use of the Limber approximation by ignoring the lens-lens coupling is not expected to change the final results significantly.

For the purpose of this calculation, we assume that the upcoming weak-lensing convergence power spectrum will measure binned logarithmic band powers at several l_i in multipole space with bins of thickness δl_i;

$$\mathscr{C}_i = \int_{s,i}\frac{d^2l}{A_{s,i}}\,\frac{l^2}{2\pi}\,\kappa(\boldsymbol{l})\kappa(-\boldsymbol{l})\,, \quad (36)$$

where $A_{s,i} = \int d^2l$ is the area of the two-dimensional shell in multipole and can be written as $A_{s,i} = 2\pi l_i\,\delta l_i + \pi(\delta l_i)^2$.

We can now write the signal covariance matrix as

$$C_{ij} = \frac{1}{A}\left[\frac{(2\pi)^2}{A_{s,i}}\,2\mathscr{C}_i^2 + T_{ij}^\kappa\right], \quad (37)$$

$$T_{ij}^\kappa = \int\frac{d^2l_i}{A_{s,i}}\int\frac{d^2l_j}{A_{s,j}}\,\frac{l_i^2\,l_j^2}{(2\pi)^2}\,T^\kappa(\boldsymbol{l}_i,-\boldsymbol{l}_i,\boldsymbol{l}_j,-\boldsymbol{l}_j)\,, \quad (38)$$

where A is the area of the survey in steradians. Again, the first term is the Gaussian contribution to the sample variance and the second is the non-Gaussian contribution. A realistic survey will also have shot noise variance due to the finite number of source galaxies in the survey. We return to this point in § 3.3.

3.2. *Comparisons*

Using the halo model, we can now calculate contributions to the lensing convergence power spectrum and trispectrum. The logarithmic power spectrum, shown in Figure 4*a*, shows the same behavior as the density field when compared with the PD results: a slight overprediction of power when $l \gtrsim 10^3$. However, these differences are not likely to be observable, given the shot noise from the finite number of galaxies at small scales.

In Figure 4*b* we show the scaled trispectrum,

$$\Delta_{\rm sq}^\kappa(l) = \frac{l^2}{2\pi}\,T^\kappa(\boldsymbol{l},-\boldsymbol{l},\boldsymbol{l}_\perp,-\boldsymbol{l}_\perp)^{1/3}\,. \quad (39)$$

where $l_\perp = l$ and $\boldsymbol{l}\cdot\boldsymbol{l}_\perp = 0$. The projected lensing trispectrum again shows the same behavior as the density field trispectrum with similar conditions on $\boldsymbol{k}_i$.

We can now use this trispectrum to study the contributions to the covariance, which is what primarily concerns us

here. In Figure 5*a* we show the fractional error,

$$\frac{\Delta \mathscr{C}_i}{\mathscr{C}_i} \equiv \frac{\sqrt{C_{ii}}}{\mathscr{C}_i}, \tag{40}$$

for bands l_i given in Table 2 following the binning scheme used by White & Hu (2000) on $6^\circ \times 6^\circ$ fields. The dashed line compares that with the Gaussian errors, involving the first term in the covariance (eq. [38]). At multipoles of a few hundred and greater, the non-Gaussian term begins to dominate the contributions. For this reason, the errors are well approximated by simply taking the Gaussian and single-halo contributions.

In Figure 5*b*, we compare these results with those of the White & Hu (2000) simulations. The decrease in errors from the simulations at small l reflects finite box effects that convert variance to covariance as the fundamental mode in the box becomes comparable to the bandwidth.

The correlation between the bands is given by

$$\hat{C}_{ij} \equiv \frac{C_{ij}}{\sqrt{C_{ii} C_{jj}}}. \tag{41}$$

In Table 2 we compare the halo predictions to the simulations by White & Hu (2000). The upper triangle here gives the correlations under the halo approach, while the lower triangle shows the correlations found in numerical simulations. The correlations along individual columns increase (as one goes to large l or small angular scales), consistent with simulations. In Figures 6*a* and 6*b* we show the correlation coefficients with and without the Gaussian contribution to the diagonal, respectively.

Figure 6*a* shows the behavior of the correlation coefficient between a fixed l_j as a function of l_i. When $l_i = l_j$ the coefficient is 1 by definition. Because of the presence of the dominant Gaussian contribution at $l_i = l_j$, the coefficient has an apparent discontinuity between $l_i = l_j$ and $l_i = l_{j-1}$ that decreases as l_j increases and non-Gaussian effects dominate.

To better understand this behavior, it is useful to isolate the purely non-Gaussian correlation coefficient,

$$\hat{C}^{\rm NG}_{ij} = \frac{T_{ij}}{\sqrt{T_{ii} T_{ij}}}. \tag{42}$$

As shown in Figure 6*b*, the coefficient remains constant for $l_i \ll l_j$ and smoothly increases to unity across a transition scale that is related to where the single-halo terms starts to contribute. A comparison of Figures 6*b* and 4*b* shows that this transition happens around l of few hundred to 1000. Once the power spectrum is dominated by correlations in single halos, the fixed profile of the halos will correlate the power in all the modes. The multiple halo terms, on the other hand, correlate linear and nonlinear scales but at a level that is generally negligible compared to the Gaussian variance.

The behavior seen in the halo based covariance, however, is not present when the covariance is calculated with hierarchical arguments for the trispectrum (see Scoccimarro et al. 1999). With hierarchical arguments, which are by construction only valid in the deeply nonlinear regime, one predicts correlations that are, in general, constant across all scales and show no decrease in correlations between very small and very large scales. Such hierarchical models also violate the Schwarz inequality with correlations greater than 1 between large and small scales (e.g., Scoccimarro et al. 1999; Hamilton 2000). The halo model, however, shows a decrease in correlations similar to numerical simulations, suggesting that the halo model, at least qualitatively, provides a better approach to studying non-Gaussian correlations in the translinear regime.

3.3. *Effect on Parameter Estimation*

Modeling or measuring the covariance matrix of the power spectrum estimates will be essential for interpreting observational results. In the absence of many fields where the covariance can be estimated directly from the data, the halo model provides a useful, albeit model-dependent, quantification of the covariance. As a practical approach, one could imagine taking the variances estimated from the survey under a Gaussian approximation, but which accounts for uneven sampling and edge effects (Hu & White 2000), and scaling it up by the non-Gaussian to Gaussian variance ratio of the halo model, along with the inclusion of the band-power correlations. In addition, it is in principle possible to use the expected correlations from the halo model to decorrelate individual band-power measurements, similar to studies involving CMB temperature anisotropy and galaxy power spectra (e.g., Hamilton 1997; Hamilton & Tegmark 2000).

We can estimate the resulting effects on cosmological parameter estimation with an analogous procedure on the Fisher matrix. In Hu & Tegmark (1999), the potential of

TABLE 2

WEAK-LENSING CONVERGENCE POWER SPECTRUM CORRELATIONS

$l_{\rm bin}$	97	138	194	271	378	529	739	1031	1440	2012
97	1.00	0.04	0.05	0.07	0.08	0.09	0.09	0.09	0.08	0.08
138	(0.26)	1.00	0.08	0.10	0.11	0.12	0.12	0.12	0.11	0.11
194	(0.12)	(0.31)	1.00	0.14	0.17	0.18	0.18	0.17	0.16	0.15
271	(0.10)	(0.21)	(0.26)	1.00	0.24	0.25	0.25	0.24	0.22	0.21
378	(0.02)	(0.09)	(0.24)	(0.38)	1.00	0.33	0.33	0.32	0.30	0.28
529	(0.10)	(0.14)	(0.28)	(0.33)	(0.45)	1.00	0.42	0.40	0.37	0.35
739	(0.12)	(0.16)	(0.17)	(0.34)	(0.38)	(0.50)	1.00	0.48	0.45	0.42
1031.....	(0.15)	(0.18)	(0.15)	(0.27)	(0.33)	(0.48)	(0.54)	1.00	0.52	0.48
1440.....	(0.18)	(0.15)	(0.19)	(0.19)	(0.32)	(0.36)	(0.53)	(0.57)	1.00	0.54
2012.....	(0.19)	(0.22)	(0.16)	(0.32)	(0.27)	(0.46)	(0.50)	(0.61)	(0.65)	1.00

NOTE.—Covariance of the binned power spectrum when sources are at a redshift of 1. Upper triangle displays the covariance found under the halo model. Lower triangle (parenthetical numbers) displays the covariance found in numerical simulations by White & Hu 2000. To be consistent with these simulations, we use the same binning scheme as the one used there.

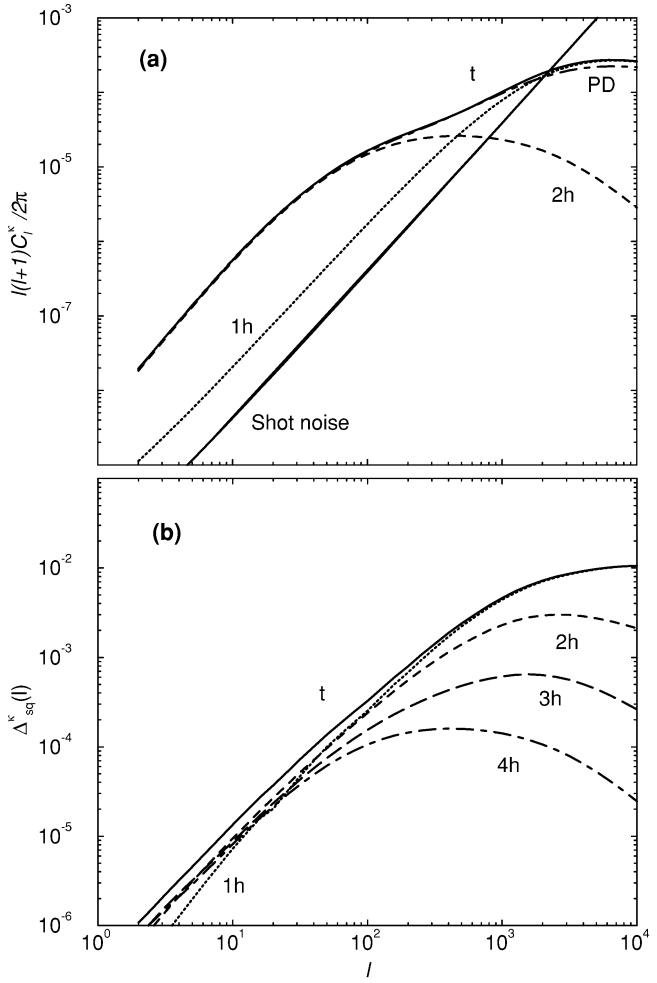

FIG. 4.—Weak-lensing convergence (*a*) power spectrum and (*b*) trispectrum under the halo description. Also shown in (*a*) is the prediction from the PD nonlinear power spectrum fitting function. We have separated individual contributions under the halo approach and have assumed that all sources are at $z_s = 1$. We also show the shot-noise contribution to the power spectrum assuming a survey down to a limiting magnitude of $R \sim 25$ with an intrinsic rms shear of 0.4 in each component.

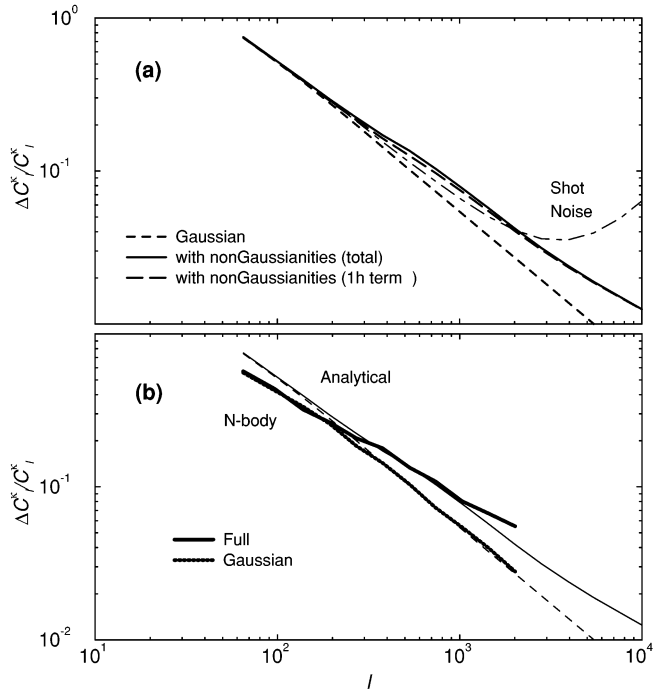

FIG. 5.—Fractional errors in the measurements of the convergence band powers. (*a*) Fractional errors under the Gaussian approximation, the full halo description, the Gaussian plus single halo term, and the Gaussian plus shot noise term (see § 3.3). As shown, the additional variance can be modeled with the single halo piece, while shot noise generally becomes dominant before non-Gaussian effects become large. In (*b*), we compare the halo model with simulations from White & Hu (2000). The decrease in the variance at small l in the simulations is due to the conversion of variance to covariance by the finite box size of the simulations.

wide-field lensing surveys to measure cosmological parameters was investigated using the Gaussian approximation of a diagonal covariance and Fisher matrix techniques. The Fisher matrix is simply a projection of the covariance matrix onto the basis of cosmological parameters p_i,

$$\boldsymbol{F}_{\alpha\beta} = \sum_{ij} \frac{\partial \mathscr{C}_i}{\partial p_\alpha} (C_{\rm tot}^{-1})_{ij} \frac{\partial \mathscr{C}_j}{\partial p_\beta}\,, \tag{43}$$

where the total covariance includes both the signal and noise covariance. Under the approximation of Gaussian shot noise, this reduces to replacing $C_l^\kappa \to C_l^\kappa + C_l^{\rm SN}$ in the expressions leading up to the covariance equation (38). The shot-noise power spectrum is given by

$$C_l^{\rm SN} = \frac{\langle \gamma_{\rm int}^2 \rangle}{\bar{n}}\,, \tag{44}$$

where $\langle \gamma_{\rm int} \rangle^{1/2} \sim 0.4$ is the rms noise per component introduced by intrinsic ellipticities and measurement errors, and $\bar{n} \sim 6.6 \times 10^8$ sr^{-1} is the surface number density of background source galaxies. The numerical values here are appropriate for surveys that reach a limiting magnitude in $R \sim 25$ (e.g., Smail et al. 1995).

Under the approximation that there are a sufficient number of modes in the band powers that the distribution of power spectrum estimates is approximately Gaussian, the Fisher matrix quantifies the best possible errors on cosmological parameters that can be achieved by a given survey. In particular, F^{-1} is the optimal covariance matrix of the parameters and $(F^{-1})_{ii}^{1/2}$ is the optimal error on the ith parameter. Implicit in this approximation of the Fisher matrix is a neglect of information from the cosmological parameter dependence of the covariance matrix of the band powers themselves. Since the covariance is much less than the mean power, we expect this information content to be small.

In order to estimate the effect of non-Gaussianities on the cosmological parameters, we calculate the Fisher matrix elements using our fiducial ΛCDM cosmological model and define the dark matter density field today as

$$\Delta^2(k) = A^2 \left(\frac{k}{H_0}\right)^{n_s+3} T^2(k)\,, \tag{45}$$

where A is the amplitude of the present-day density fluctuations and n_s is the tilt at the Hubble scale. The density power spectrum is evolved to higher redshifts using the growth function $G(z)$ (Peebles 1980), and the transfer function $T(k)$ is calculated using the fitting functions from Eisenstein & Hu (1999). Since we are only interested in the relative effect of non-Gaussianities, we restrict ourselves to a small subset of the cosmological parameters considered

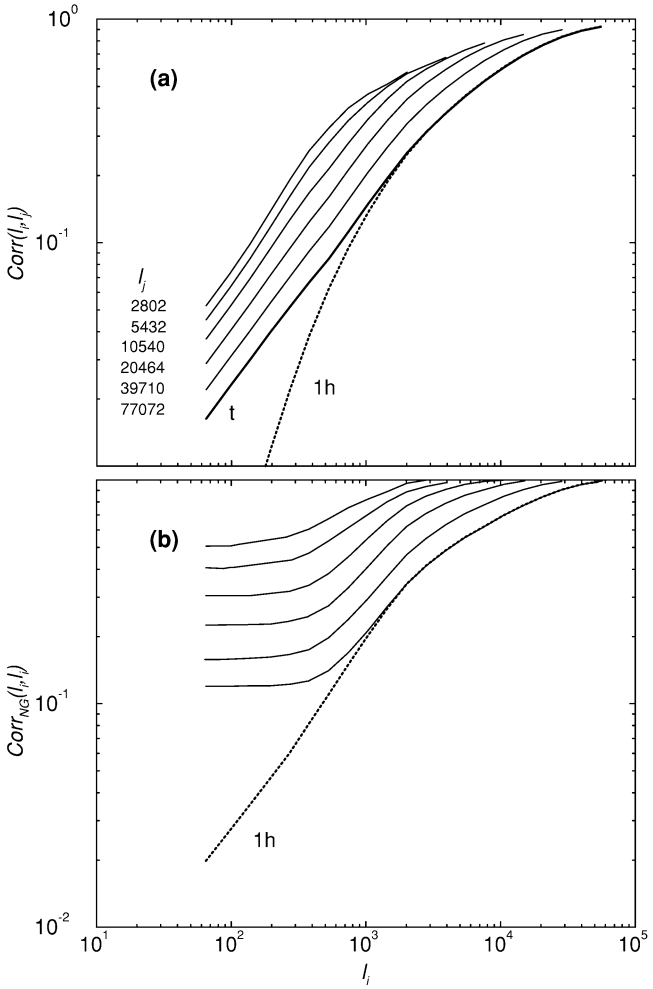

FIG. 6.—(*a*) Correlation coefficient, $\hat{C}_{ij}$, as a function of the multipole l_i with l_j as shown in the figure. We show the correlations calculated with the full halo model and also with only the single halo term for $l_j = 77072$. (*b*) Non-Gaussian correlation coefficient, $\hat{C}_{ij}^{\rm NG}$, which only involves the trispectrum (see eq. [42]). The transition to full correlation is due to the domination of the single halo contribution.

by Hu & Tegmark (1999) and assume a full-sky survey with $f_{\rm sky} = 1$.

In Table 3, we show the inverse Fisher matrices determined under the Gaussian and non-Gaussian covariances, respectively. For the purpose of this calculation, we adopt the binning scheme as shown in Table 2, following White & Hu (2000). The Gaussian errors are computed using the same scheme by setting $T^{\kappa} = 0$. As shown in Table 3, the inclusion of non-Gaussianities leads to an increase in the inverse Fisher matrix elements. We compare the errors on individual parameters, mainly $(F^{-1})_{ii}^{1/2}$, between the Gaussian and non-Gaussian assumptions in Table 4. The errors increase typically by $\sim$15%. Note also that band-power correlations do not necessarily increase cosmological parameter errors. Correlations induced by nonlinear gravity introduce larger errors in the overall amplitude of the power spectrum measurements but have a much smaller effect on those parameters controlling the shape of the spectrum.

For a survey of this assumed depth, the shot-noise power becomes the dominant error before the non-Gaussian signal effects dominate over the Gaussian ones. For a deeper survey with better imaging, such as the one planned with the Large-Aperture Synoptic Survey Telescope (LSST; Tyson & Angel 2000),[4] the effect of shot noise decreases and non-Gaussianity is potentially more important. However, the non-Gaussianity itself also decreases with survey depth, and, as we now discuss, in terms of the effect of non-Gaussianities, deeper surveys should be preferred over shallow ones.

TABLE 3

INVERSE FISHER MATRIX ($\times 10^3$)

A: Gaussian Assumption

p_i	Ω_Λ	ln A	Ω_K	n_s	$\Omega_m h^2$
Ω_Λ	1.57	−5.96	−1.39	4.41	−1.76
ln A		25.89	5.83	−17.34	6.74
Ω_K			1.41	−3.81	1.43
n_s				14.01	−6.03
$\Omega_m h^2$					2.67

B: Halo Model

p_i	Ω_Λ	ln A	Ω_K	n_s	$\Omega_m h^2$
Ω_Λ	2.03	−7.84	−1.82	5.76	−2.30
ln A		33.92	7.65	−22.79	8.91
Ω_K			1.78	−5.01	1.95
n_s				18.43	−7.85
$\Omega_m h^2$					3.44

NOTE.—Inverse Fisher matrix under the Gaussian assumption (A) and the halo model (B). The error on an individual parameter is the square root of the diagonal element of the Fisher matrix for the parameter, while off-diagonal entries of the inverse Fisher matrix show correlations, and thus degeneracies, between parameters. We have assumed a full-sky survey ($f_{\rm sky} = 1$) with parameters as described in § 3.3.

3.4. *Scaling Relations*

To better understand how the non-Gaussian contribution scales with our assumptions, we consider the ratio of non-Gaussian variance to Gaussian variance (Scoccimarro et al. 1999),

$$\frac{C_{ii}}{C_{ii}^{\rm G}} = 1 + R\,, \tag{46}$$

with

$$R \equiv \frac{A_{s,i}\, T_{ii}^{\kappa}}{(2\pi)^2 2 C_i^2}\,. \tag{47}$$

Under the assumption that contributions to lensing convergence can be written through an effective distance r_*, at

[4] Large-Aperture Synoptic Survey Telescope is available at: http://www.dmtelescope.org.

TABLE 4

PARAMETER ERRORS

Model	Ω_Λ	ln A	Ω_k	n_s	$\Omega_m h^2$
Gaussian	0.039	0.160	0.037	0.118	0.051
Full	0.045	0.184	0.042	0.135	0.058
Increase (%).....	15.3	15	13.5	14.4	13.7

NOTE.—Parameter errors, $(F^{-1})_{ii}^{1/2}$, under the Gaussian assumption and the halo model, and following the inverse-Fisher matrices in Table 3. We have assumed a full-sky survey ($f_{\rm sky} = 1$) with parameters as described in § 3.3.

half the angular diameter distance to background sources, and a width Δr for the lensing window function, the ratio of lensing convergence trispectrum and power spectrum contribution to the variance can be further simplified to

$$R \sim \frac{A_{s,i}}{(2\pi)^2 V_{\rm eff}} \frac{\bar{T}(r_*)}{2\bar{P}^2(r_*)} . \quad (48)$$

Since the lensing window function peaks at r_*, we have replaced the integral over the window function of the density field trispectrum and power spectrum by its value at the peak. This ratio shows how the relative contribution from non-Gaussianities scales with survey parameters: (1) increasing the bin size, through $A_{s,i}$ ($\propto \delta l$), leads to an increase in the non-Gaussian contribution linearly; (2) increasing the source redshift, through the effective volume of lenses in the survey ($V_{\rm eff} \sim r_*^2 \Delta r$), decreases the non-Gaussian contribution; while (3) the growth of the density field trispectrum and power spectrum, through the ratio $\bar{T}/\bar{P}^2$, decreases the contribution as one moves to a higher redshift. The volume factor quantifies the number of foreground halos in the survey that effectively act as gravitational lenses for background sources; as the number of such halos is increased, the non-Gaussianities are reduced by the central limit theorem.

In Figure 7, we summarize our results as a function of source redshift with $l_i \sim 10^2$, 10^3, and 10^4, and setting the bin width such that $A_{s,i} \sim l_i^2$, or $\delta l \sim l$. As shown, increasing the source redshift leads to a decrease in the non-Gaussian contribution to the variance. The predictions based on the simplifications in equation (48) tend to overestimate the non-Gaussianity at lower redshifts while underestimating it at higher redshifts, although the exact transition depends on the angular scale of interest; this behavior can be understood from the fact that we do not consider the full lensing window function but only the contributions at an effective redshift, midway between the observer and sources.

In order to determine whether it is the increase in volume or the decrease in the growth of structures that leads to a decrease in the relative importance of non-Gaussianities as one moves to a higher source redshift, we calculated the non-Gaussian to Gaussian variance ratio under the halo model for several source redshifts and survey volumes. Up to source redshifts ~ 1.5, the increase in volume decreases the non-Gaussian contribution significantly. When surveys are sensitive to sources at redshifts beyond 1.5, the increase in volume becomes less significant, and the decrease in the growth of structures begins to be important in decreasing the non-Gaussian contribution. Since in the deeply nonlinear regime $\bar{T}/\bar{P}^2$ scales with redshift as the cube of the growth factor, this behavior is consistent with the overall redshift scaling of the volume and growth.

The importance of the non-Gaussianity to the variance also scales linearly with bin width. As one increases the bin width, the covariance induced by the non-Gaussianity manifests itself as increased variance relative to the Gaussian case. The normalization of R is therefore somewhat arbitrary in that it depends on the binning scheme, i.e., $R \ll 1$ does not necessarily mean non-Gaussianity can be entirely neglected when summing over all the bins. The scaling with redshift and the overall scaling of the variance with the survey area A is not. One way to get around the increased non-Gaussianity associated with shallow surveys is to have them sample a wide patch of sky, since $C_{ii} \propto (1 + R)/A$. This relation tells us the trade-off between designing a survey to go wide instead of deep. One should bear in mind, however, that not only will shallow surveys have decreasing number densities of source galaxies, and hence increasing shot noise, but they will also suffer more from the decreasing amplitude of the signal itself and the increasing importance of systematic effects, including the intrinsic correlations of galaxy shapes (e.g., Catelan, Kamionkowski, & Blandford 2001; Croft & Metzler 2000; Heavens, Refregier, & Heymans 2000). These problems tilt the balance more toward deep but narrow surveys than the naive statistical scaling would suggest.

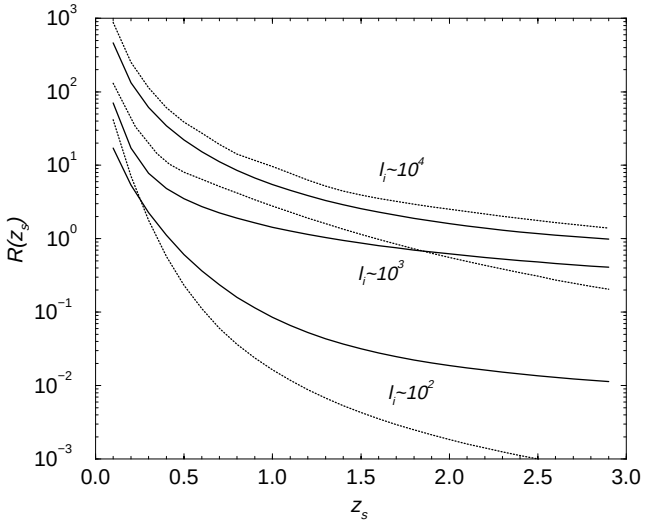

FIG. 7.—Ratio of non-Gaussian to Gaussian contributions, R, as a function of source redshift (z_s). The solid lines are generated through the exact calculation (eq. [47]), while the dotted lines use the approximation given in eq. (48). Here we show the ratio R for three multipoles corresponding to large, medium, and small angular scales. The multipole binning is kept constant, such that $\delta l \sim l$. Decreasing this bin size will linearly decrease the value of R.

4. CONCLUSIONS

Weak gravitational lensing due to large-scale structure provides important information on the evolution of clustering and angular diameter distances, and therefore on cosmological parameters. This information complements what can be learned from cosmic microwave background anisotropy observations. The tremendous progress on the observational front warrants detailed studies of the statistical properties of the lensing observables and their use in constraining cosmological models.

The nonlinear growth of large-scale structure induces high-order correlations in the derived shear and convergence fields. In this work, we have studied the four-point correlations in the fields. Four-point statistics are special in that they quantify the errors in the determination of the two-point statistics. To interpret future lensing measurements on the power spectrum, it will be essential to have an accurate assessment of the correlation between the measurements.

Using the halo model for clustering, we have provided a semianalytical method to calculate the four-point function of the lensing convergence, as well as the dark matter density field. We have tested this model against numerical N-body simulations of the power spectrum covariance in

both the density and convergence fields and obtained good agreement. As such, this method provides a practical means of estimating the error matrix from future surveys in the absence of sufficiently large fields, where it can be estimated directly from the data, or large suites of N-body simulations, where it can be quantified in a given model context. Eventually, a test of whether the covariance matrix estimated from the data and the theory agree may even provide further cosmological constraints.

This method can also be used to study other aspects of the four-point function in lensing and any field whose relation to the dark matter density field can be modeled. Given the approximate nature of these models, each potential use must be tested against simulations. Nonetheless, the halo model provides the most intuitive and extensible means to study non-Gaussianity in the cosmological context currently known.

We acknowledge useful discussions with Dragan Huterer, Roman Scoccimaro, Uros Seljak, Ravi Sheth, and Matias Zaldarriaga. W. H. is supported by the Alfred P. Sloan Foundation.

REFERENCES

Bacon, D., Refregier, A., & Ellis R. 2000, MNRAS, 318, 625
Bartelmann, M., & Schneider, P. 2001, Phys. Rep., 340, 291
Bernardeau, F., van Waerbeke, L., & Mellier, Y. 1997, A&A, 322, 1
Blandford, R. D., Saust, A. B., Brainerd, T. G., & Villumsen, J. V. 1991, MNRAS, 251, 600
Bullock, J. S., et al. 2001, MNRAS, 321, 559
Bunn, E. F., & White, M. 1997, ApJ, 480, 6
Catelan, P., Kamionkowski, M., & Blandford, R. D. 2001, MNRAS, 320, 7L
Cooray, A. R. 1999, A&A, 348, 673
Cooray, A., & Hu, W. 2001, ApJ, 548, 7
Cooray, A., Hu, W., & Miralda-Escudé, J. 2000, ApJ, 535, L9
Croft, R. A., & Metzler, C. 2000, ApJ, 545, 561
Eisenstein, D. J., & Hu, W. 1999, ApJ, 511, 5
Eisenstein, D. J., & Zaldarriaga, M. 2001, ApJ, 546, 2
Fry, J. N. 1984, ApJ, 279, 499
Goroff, M. H., Grinstein, B., Rey, S.-J., & Wise, M. 1986, ApJ, 311, 6
Hamilton, A. J. S. 1997, MNRAS, 289, 285
———. 2000, MNRAS, 312, 257
Hamilton, A. J. S., & Tegmark, M. 2000, MNRAS, 312, 285
Heavens, A., Refregier, A., & Heymans, C. 2000, MNRAS, 319, 649
Hu, W., & Tegmark, M. 1999, ApJ, 514, L65
Hu, W., & White, M. 2000, ApJ, in press (preprint astro-ph/0010352)
Hui, L. 1999, ApJ, 519, L9
Jain, B., & Seljak, U. 1997, ApJ, 484, 560
Jain, B., Seljak, U., & White, M. 2000, ApJ, 530, 547
Kaiser, N. 1992, ApJ, 388, 272
———. 1998, ApJ, 498, 26
Kaiser, N., Wilson, G., & Luppino, G. A. 2000, ApJL, submitted (preprint astro-ph/0003338)
Limber, D. 1954, ApJ, 119, 655
Ma, C.-P., & Fry, J. N. 2000a, ApJ, 543, 503
———. 2000b, ApJ, 538, L107
Meiksin, A., & White, M. 1999, MNRAS, 308, 1179
Miralda-Escudé, J. 1991, ApJ, 380, 1
Mo, H. J., Jing, Y. P., & White, S. D. M. 1997, MNRAS, 284, 189
Navarro, J., Frenk, C., & White, S. D. M. 1996, ApJ, 462, 563 (NFW)
Peacock, J. A., & Dodds, S. J. 1996, MNRAS, 280, L19
Peebles, P. J. E. 1980, The Large-Scale Structure of the Universe (Princeton: Princeton Univ. Press)
Press, W. H., & Schechter, P. 1974, ApJ, 187, 425 (PS)
Schneider, P., van Waerbeke, L., Jain, B., & Guido, K. 1998, MNRAS, 296, 873
Scoccimarro, R., & Frieman, J. 1999, ApJ, 520, 35
Scoccimarro, R., Sheth, R., Hui, L., & Jain, B. 2001, ApJ, 546, 20
Scoccimarro, R., Zaldarriaga, M., & Hui, L. 1999, ApJ, 527, 1
Seljak, U. 2000, MNRAS, 318, 203
Smail, I., Hogg, S. W., Yan, L., & Cohen, J. G. 1995, ApJ, 449, L105
Tyson, A., & Angel, R. 2001, in ASP Conf. Ser. 232, The New Era of Wide-Field Astronomy, ed. R. Clowes, A. Adamson, & G. Bromage (San Francisco: ASP), in press
Van Waerbeke, L., Bernardeau, F., & Mellier, Y. 1999, A&A, 342, 15
Van Waerbeke, L., Hamana, T., Scocimarro, R., Colombi, S., & Bernardeau, F. 2001, MNRAS, 322, 918
Van Waerbeke, L., et al. 2000, A&A, 358, 30
Viana, P. T. P., & Liddle, A. R. 1999, MNRAS, 303, 535
White, M., & Hu, W. 2000, ApJ, 537, 1
Wittman, D. M., Tyson, J. A., Kirkman, D., Dell'Antonio, I., & Bernstein, G. 2000, Nature, 405, 143